6-15-2014

Effect of Accelerated Carbonation on AOD Stainless Steel Slag for Its Valorisation as a CO2-sequestering Construction Material

Rafael M. Santos
Katholieke Universiteit Leuven, rafael.santos@sheridancollege.ca

Muhammad Salman
Katholieke Universiteit Leuven

Özlem Cizer
Katholieke Universiteit Leuven

Yiannis Pontikes
Katholieke Universiteit Leuven

Ruben Snellings
Ecole Polytechnique Fédérale de Lausanne

See next page for additional authors

Authors
Rafael M. Santos, Muhammad Salman, Özlem Cizer, Yiannis Pontikes, Ruben Snellings, Lucie Vandewalle, Bart Blanpain, and Koen van Balen

Effect of accelerated carbonation on AOD stainless steel slag for its valorisation as a CO_2-sequestering construction material

Muhammad Salman, Özlem Cizer, Yiannis Pontikes, Rafael M Santos, Ruben Snellings, Lucie Vandewalle, Bart Blanpain, Koen van Balen

PII: S1385-8947(14)00199-5
DOI: http://dx.doi.org/10.1016/j.cej.2014.02.051
Reference: CEJ 11798

To appear in: *Chemical Engineering Journal*

Received Date: 29 November 2013
Revised Date: 13 February 2014
Accepted Date: 15 February 2014

Please cite this article as: M. Salman, Ö. Cizer, Y. Pontikes, R.M. Santos, R. Snellings, L. Vandewalle, B. Blanpain, K. van Balen, Effect of accelerated carbonation on AOD stainless steel slag for its valorisation as a CO_2-sequestering construction material, *Chemical Engineering Journal* (2014), doi: http://dx.doi.org/10.1016/j.cej.2014.02.051

Effect of accelerated carbonation on AOD stainless steel slag for its valorisation as a CO_2-sequestering construction material

Muhammad Salman[a,*], Özlem Cizer[a], Yiannis Pontikes[b], Rafael M Santos[c], Ruben Snellings[d], Lucie Vandewalle[a], Bart Blanpain[b], Koen van Balen[a]

[a]KU Leuven, Department of Civil Engineering, Kasteelpark Arenberg 40, 3001 Leuven, Belgium

[b]KU Leuven, High Temperature Processes and Industrial Ecology, Department of Metallurgy and Materials Engineering, Kasteelpark Arenberg 44, 3001 Leuven, Belgium

[c]KU Leuven, Department of Chemical Engineering, Willem de Croylaan 46, 3001 Leuven, Belgium

[d]Ecole Polytechnique Fédérale de Lausanne, Laboratory of Construction Materials, Institute of Materials, MXG 234, Station 12, 1015 Ecublens, Switzerland

Corresponding author:

Email: muhammad.salman@bwk.kuleuven.be

Tel: +32 16 32 1678
Fax: +32 16 32 1976

Abstract

Non-stabilized Argon Oxygen Decarburisation (AODNS) slag in powdered form was examined for its carbon dioxide sequestration capacity and for its potential utilization in the fabrication of high value building materials. The curing of the sample was carried out in two accelerated carbonation environments: i) in a carbonation chamber, maintained at atmospheric pressure, 22 °C, 5 vol.% CO_2 and 80% RH; and ii) in a carbonation reactor, where the CO_2 partial pressure (pCO_2) and temperature could be further increased. In the carbonation chamber, an average compressive strength of over 20 MPa, on a 64 cm^3 cubic specimen, was obtained after one week of curing, which is sufficient for many construction applications. Further carbonation resulted in a linear increase of strength up ~30 MPa after three weeks. The CO_2 uptake followed a similar trend, reaching a maximum of 4.3 wt.%. In the reactor, the compressive strength improved with an increase in pCO_2 up to 8 bar, temperature up to 80 °C, and duration up to 15 h where the maximum CO_2 uptake was 8.1 wt%. The reduction in porosity in the carbonated specimens was approximately in line with the strength gain in the samples. Phase analysis by X-ray powder diffraction and inspection by scanning electron microscopy showed the precipitation of calcite and formation of significant amounts of amorphous material after carbonation. Infrared spectroscopy also pointed to the presence of aragonite and vaterite. In the carbonation chamber, the calcite morphology was uniform throughout the specimen. In the reactor, however, the calcite crystals near the outer edges of the cubes had different morphology than those near the core. Carbonation of the slag resulted in the reduction of basicity by up to one pH unit, and contributed to controlling the leaching of several heavy metals and metalloids.

Keywords: AOD slag; Mineral carbonation; Compressive strength; Mineralogy analysis; Microstructure; Leaching

1. Introduction

Mineral carbonation deals with the capture and fixation of carbon dioxide (CO_2) in the form of inorganic carbonates and it is part of the carbon capture and storage (CCS) scheme. The Intergovernmental Panel on Climate Change (IPCC) considers CCS as an important option among the portfolio of mitigation actions under consideration for the stabilization of atmospheric greenhouse gas concentrations [1]. The usual materials for mineral carbonation are calcium and magnesium rich oxides and silicates which can form solid carbonate products [2]. A key driver for the viability of mineral carbonation is the availability of such materials in the vicinity of anthropogenic CO_2 source. A suitable class of materials are alkaline slags generated as by-products from steel producing industries, which in turn are heavy CO_2 emitters [3]. The potential carbon credits to be gained by the utilization of these slags for CO_2 capture, coupled with the transformation of these burdensome low-value waste residues into high added value marketable end-products, can result in an economically favourable industrial CCS process.

Several research works have demonstrated the potential of steel slags for the sequestration of CO_2. The common slags used for this purpose are: basic oxygen furnace (BOF) steel slag - generated during primary steelmaking; electric arc furnace (EAF) slag - generated during the melting of scrap carbon or stainless steel; argon oxygen decarburisation (AOD) slag - generated during the refining of stainless steel and continuous casting (CtCs) slag - generated during the final stage of the stainless steel production process. Chang et. al. [4, 5] showed that high CO_2 sequestration can be achieved in finely milled BOF slag in a slurry reactor and Santos et. al. [6] demonstrated the feasibility of CO_2 sequestration in BOF slag as it cools down from its high temperature origin. Baciocchi et. al. [7, 8] reported that milled EAF slag

can be carbonated by wet and slurry-phase carbonation process and that of the two routes, the wet process is more effective.

Whereas BOF and EAF slags are typically morphologically stable solids (i.e. primarily granular and monolithic shaped), the physical form of untreated AOD and CtCs slags is that of a fine powder. This is caused by the presence of a large amount of dicalcium silicate (C_2S) in the slag, which undergoes polymorphic transformations while cooling, the most important of which is the $\beta \rightarrow \gamma$ polymorph transformation that occurs near 500 °C and is accompanied by a volumetric slag expansion of ~ 12% [9]. This phenomenon results in pulverisation of the slag into fine powder, a process referred as dusting. This makes the handling of the slag difficult in the steel industry. In order to avoid the problem of dusting, boron can be added to the slag while in the molten state to stabilize the C_2S in the β-form, thus preventing the formation of fines [10, 11]. Such stabilised slag along with other crushed/milled slags can then be used as aggregates, mostly in road construction. However, the use as a road aggregate is a low-value application for the slag. Moreover, boron additions also increases the risk of leaching, posing a further environmental challenge for the use of this slag.

Fine slag has the inherent advantage that no energy intensive milling is required for their effective carbonation. Baciocchi et. al. [7] have demonstrated that even under mild operating conditions of temperature and pressure, carbonation of humidified AOD slag is possible. In another study, Santos et. al. [12, 13] have shown that carbonation of AOD and CtCs slags can be achieved through a variety of processes that include ultrasonic-intensification, thin film and slurry carbonation. The resulting carbonated granules can be potentially valorised as building materials for the construction industry. Yet, the resulting carbonated materials, from the aforementioned works is either left unvalorised, or have a low valorisation potential (e.g. as fine aggregates). Carbonation processes are in themselves cost demanding, as several

intensification strategies are needed to achieve satisfactory results. Hence, high-value end-products are desirable, as this not only maximizes the investment return, but also aids in the effective recycling of the waste residues replacing primary resources, and hence contributing to the sustainability of the industry.

The fact that the carbonation of alkaline earth metal oxides/hydroxides has the ability to form strong, stable and durable carbonates has been historically demonstrated bythe successful use of slaked lime ($Ca(OH)_2$) as binder in masonry mortars (i.e. lime mortar), found in traditional Greek and Roman structures. $Ca(OH)_2$ reacts with atmospheric CO_2 to form calcium carbonates which impart strength to the masonry structures. However, the development of strength of this type of binder is traditionally slow and uneven due to the low partial pressure of CO_2 in the atmosphere (presently ~0.04 vol.%) and the slow diffusion of CO_2 into the mortar [14]. This led to the development of new binders, the most common of which is ordinary Portland cement (OPC). The uptake of CO_2 in this binder during application is, however, very limited; rather, its production contributes to net positive CO_2 emissions.

Currently, the production of OPC generates about 5-8% of the total global anthropogenic CO_2 emissions [15, 16]. Consequently, the "Cement and Technology Roadmap 2009" has laid a task for the reduction of global CO_2 emissions by the sector to 50% by 2050 [17]. As a result, cement producers around the world are tasked with finding alternative sources of binders. Alternatively, to off-set the CO_2 generated during cement production, the use of CO_2-sequestering building blocks could also improve the sustainability of the sector. Carbonation-prone materials with binding and strength-gaining abilities would be an effective contributor for this goal.

Besides sequestering CO_2, carbonation of waste residues also aids in reducing the leaching of several hazardous elements. In the case of EAF slag accelerated carbonation with varied

moisture content has been reported to decrease the leaching of certain heavy metals [18]. In other works, reduction in the basicity and improvement of the leaching properties of municipal solid waste incineration bottom ashes (MSWI-BA) [19, 20] and reduction in the free lime content of BOF slag [6, 21] has been achievedby various carbonation processes.

The work presented in this paper has focussed on producing clinker-free binding materials (i.e. binder) from non-stabilised AOD (AODNS) slag. The slag was used to prepare cubical compacted specimens at low water-solid ratio, representing block masonry, where carbonation acts to provide strength development and curbs the slag's leaching propensity, and where the end-product serves as a construction material as well as a carbon sink.

2. Materials and methods

The AODNS slag for the current work was obtained from a Belgian stainless steel plant and was sieved with a 500 μm sieve. The oversized material (~10 wt.%) which consisted of large particles and several metal pieces, was discarded. This fraction can, however, be used for metal recovery as it has much higher metal content per unit volume of slag compared to the original material. The undersized slag (AODNS_500) was used for the carbonation experiments.

The elemental and oxide composition of the slag (for both un-carbonated and carbonated samples) was determined by X-Ray Fluorescence (XRF) spectrometry using a Philips PW 2400 automatic sequential wavelength dispersive XRF spectrometer and quantified using Super-Q software. The mineral composition was determined by quantitative X-ray diffraction (QXRD) analysis. The data were collected on a Philips Analytical PW 1710 diffractometer with CuKα radiation (λ=1.54 Å) operating at 45 kV and 35 mA. The samples were scanned over a range of 10° to 70° 2θ. A 10 wt% ZnO internal standard was added to the samples to determine the amorphous phase content. Phase identification was carried out using

DiffracPlus EVA software. Topas Academic v4.1 [22] software was used for Rietveld refinement quantitative phase analysis. The Rietveld refinement strategy consisted of global parameters (i.e. zero error and a 5-coefficient Chebyshev background function) for each sample. The fundamental parameters approach was used to calculate peak shapes [23]. The particle density of the slag was determined by pycnometer analysis as per EN 1097-2 [24]. The particle size distribution of the slag was determined by wet laser diffraction (Malvern Mastersizer).

For the preparation of the samples for the compressive strength tests, the AODNS_500 slag was mixed with water applying a 0.15 water to slag ratio (by weight). The samples were 4 cm wide cubes and were prepared in a custom-designed mould (see Fig. S1 in the Supplementary materials) by continuous compression on a press (Schenck) at a controlled rate (10 mm/min). The bulk density of each fresh cube was 2.25 g/cm^3. Carbonation of these cubes was carried out in two accelerated carbonation environments: i) in a CO_2 chamber (Hera cell 240), operating at atmospheric pressure, 5 vol.% CO_2 concentration, 22°C and ~80% relative humidity (maintained with saturated KNO_3 salt); and ii) in a CO_2 reactor (Büchi), where the pressure and temperature could be varied (up to 20 bar and 120 °C) in a 100 vol.% CO_2 atmosphere. The compressive strength measurements on the carbonated cubes were carried out according to EN 196-1 [25] on the same apparatus used for moulding of the cubic samples. These tests were carried out at 2 mm/min, replicated on at least three samples to produce statistical data. After structural failure, the samples were oven dried at 105 °C for 12 h to remove the free moisture and then crushed in a ring mill to obtain a powder finer than 500 µm that was used for subsequent analysis.

The CO_2 uptake in the carbonated specimens was determined by thermogravimetric analysis (TGA). It was carried out using a Netzsch STA 409 PC DSC-TGA equipment operated with

flow through N_2 atmosphere (60 ml/min), at a controlled heating rate of 10 °C/min, over the temperature range of 20-1000°C. The weight loss was recorded by the TGA microbalance. The first derivative of thermogravimetry (DTG) was used to identify the reaction products based on their decomposition temperatures.

Open porosity of the carbonated cubes was determined by the water saturation test by hydrostatical weighing as per EN 1936. The pore size distribution of the carbonated cubes was determined using Mercury Intrusion Porosimetry (MIP) using Micromeritics AutoPore IV 9500 equipment. The instrument was composed of a low (3 bar) and a high (until 2000 bar) pressure unit. The contact angle of the Hg was set to 130°.

To complement XRD, TGA and DTG in the identification of carbonation reaction products, Fourier transform-infrared (FTIR) spectra of the samples were recorded on a Perkin Elmer Frontier spectrometer with an attenuated total reflection (ATR) accessory in the region of 4000–650 cm^{-1} at a resolution of 1 cm^{-1}.

The microstructural properties of the fresh and carbonated slags were assessed by scanning electron microscopy (SEM) analysis (SEM XL30, Phillips) using secondary electron mode on fractured samples, and back scatter mode on resin-mounted polished samples. For microchemical analysis, wavelength dispersive spectroscopy (WDS) was employed by means of a field emission electron microprobe (JXA-8530 F, JEOL).

Batch leaching tests were performed, in triplicates, on fresh and carbonated samples to determine the effect of carbonation on the mobility of regulated metals and on the material basicity according to standard procedure EN 12457-4/DIN 38414-S4. For each sample, an amount of 10 grams of solids was mixed with 100 ml ultrapure (18.2 MΩ cm) water (L/S = 10) in a sealed PE bottle, and shaken on a vibration table (Gerhardt Laboshake) at 160 rpm at 25 °C for 24 h. At completion, solution pH was measured to determine basicity.

Determination of aqueous elemental concentrations was performed by Inductively Coupled Plasma Mass Spectroscopy (ICP-MS, Thermo Electron X Series). The leaching solutions were diluted 20x for ICP-MS measurement; the solution matrix was 0.3 M nitric acid.

3. Results

3.1 Slag Characterisation

The oxide composition of the AODNS_500 slag is shown in Table 1. This slag is rich in CaO, which originates from the addition of lime as flux during the processing of the steel. This is followed by SiO_2, which is added during metal processing to prevent chromium oxidation and is also formed during the deoxidation of the steel, due to the reaction between oxygen and silicon dissolved in the steel. The third dominant oxide in the slag composition is MgO which originates from addition of dolomite as flux and also from the refractory lining of the furnace. Presence of CaO and MgO (62.5 wt.% total) imparts the slag its alkaline properties and reactivity towards mineral carbonation [26]. The maximum theoretical CO_2 uptake capacity of the slag attributable to CaO is 428.7 g/kg slag and to MgO is 88.2 g/kg slag, respectively resulting in a total CO_2 sequestration capacity of 516.9 g /kg slag. This corresponds to 34.1 wt% CO_2 in the carbonated material.

Complete carbonation of slags,, however, has not been reported. It has been shown, for example, that the carbonation extent of BOF slags of particle size of <38 μm at 19 bar CO_2 pressure and 100 °C can reach a maximum of 74 % of the total Ca content under slurry carbonation [27]. For the current work, the actual capacities are expected to be affected since the samples are shaped as cubes rather than free powder.

The oxides present in the AOD slag are present primarily in the form of calcium silicate and calcium-magnesium silicate phases. The respective quantities of these phases by QXRD analysis are shown in Table 2. It can be observed that C_2S [Ca_2SiO_4] in the γ-form is the

predominant phase, followed by cuspidine [$Ca_4SiO_7(F,OH)_2$], merwinite [$Ca_3Mg(SiO_4)$] and bredigite [$Ca_7Mg(SiO_4)_4$]. Periclase (MgO) and β-C_2S are also seen in smaller quantities.

The angular particle morphology of the fresh slag powder is shown in Fig. S2 (in the Supplementary materials). The slag particles consist of a variety of shapes and sizes, which can be attributed to varied mineralogy. The particle size distribution of the slag (Fig. S3 in the Supplementary materials) reveals that most of the particles in the slag are between 10-200 μm in diameter and the volume basis D_{50} of the slag is ~60 μm. The particle density of the slag determined by the pycnometer method was found to be 3.17 g/cm^3.

3.2 Compressive strength

Compressive strength is one of the most important properties of building materials and it can be related to several other mechanical and durability properties. The obtained values for the carbonated cubes prepared under different carbonation conditions are shown in Fig. 1. When accelerated carbonation was carried out in the carbonation chamber at 22 °C, atmospheric pressure, 5% CO_2 and 80% relative humidity (Fig. 1a), it was observed that the compressive strength increased over time, especially, between 3 and 7 days, when the compressive strength doubled. Thereafter further strength growth was approximately linear, reaching a maximum of 34 MPa after 21 days of carbonation. Considering that average strength of brick masonry blocks being around 15 MPa [28], carbonation for 7 days in the carbonation chamber seems sufficiently adequate to fulfil this requirement.

In the carbonation reactor, the effect of CO_2 pressure, ambient temperature and duration on the compressive strength was studied. To observe the independent influence of these parameters, the carbonation was carried out for a fixed duration of 2.5 h. The effect of pressure increase (at 20 °C) on the compressive strength of the carbonated AODNS_500 slag was not obvious (Fig. 1b). At the pressure of 4 bar, an average strength of 13.3±1.5 MPa was

achieved, which increased to 18±1.4 MPa at 8 bar. A further increase in the pressure resulted in decrease of the compressive strength. At 12, 16 and 20 bar the average strength was around 14-15 MPa. It was also found that at the pressure of 20 bar, the variability in the strength of the specimens, assessed by a number of replicates, became substantially higher (14.5±3.8 MPa).

The influence of the temperature on the compressive strength of the carbonated specimens was also studied, maintaining 8 bar CO_2 partial pressure (pCO_2) (Fig. 1c). An increase in temperature from 20 to 40 °C resulted in a statistically marginal decrease in compressive strength. Further increase to 80 °C had a positive effect on the compressive strength, though above this, at 120 °C, the inconsistency in the compressive strength values increased substantially.

The influence of carbonation time on the compressive strength was studied at 8 bar pCO_2 and 80 °C (Fig. 1d). An increase of carbonation time from 2.5 h to 5 h almost doubled the compressive strength of the carbonated specimen to 40.7 MPa, which further increased to 59.8 MPa after 15 h of carbonation. This is a notably high strength value for a monolithic material for use in standard construction applications.

3.3 Extent of CO_2 sequestration

The fractured surfaces of the carbonated slag samples after the compressive strength tests were sprayed with 1% phenolphthalein solution to observe the distribution of carbonation along the solidified matrix. Being a pH indicator, phenolphthalein exhibits a pinkish colour above pH 12, thus allows to discriminate between the uncarbonated and carbonated portions of the sample. Since carbonation results in a basicity decrease, extensively carbonated regions of the sample should show no colouration, as phenolphthalein becomes transparent below pH

12. It should be noted, however, that phenolphthalein only gives a qualitative indication of the carbonation extent.

From Fig. 2, the variation in the degree of carbonation within the samples can be observed. After 3 days of carbonation in the CO_2 chamber, the carbonation reaction reached the centre of the specimen, as indicated by the lack of colour upon phenolphthalein spray. For the specimens prepared in the carbonation reactor, at 4 bar pressure the reaction did not reach the centre within 2.5 h. Increasing the pressure to 8 and 12 bar allowed CO_2 to reach the centre. At higher pressure, however the carbonation reaction was again limited to the outer parts of the cube. The effect of temperature increase at 8 bar also resulted in the reappearance of the pink colour at the core. These results suggest that over-intensification of the carbonation reaction results in rapid carbonation at the surface of the specimen, hindering the diffusivity of CO_2 to the core. Nevertheless, after 15 h, the carbonation reaction reached the core and the sample was homogenously carbonated as indicated by the lack of colour change upon phenolphthalein spray.

The fractured specimen after 3 weeks of carbonation in the CO_2 chamber show more brittle failure than the 3 day specimen, by the presence of smaller sized pieces, indicating that failure in samples of higher compressive strength was more brittle. This was also observed with the samples carbonated in the reactor for 15 h. The different slag specimens at 20 bar and 120 °C conditions showed large variability in strength, as observed in compressive strength tests (11.2 MPa and 18.7 MPa at 20 bar and 13.5 MPa and 46.9 MPa at 120 ºC). Here the difference in strength can be visualized by the sizes of the fractured samples.

The CO_2 uptake of the cubic specimens was computed from TGA data (shown in Fig. S4 in the Supplementary materials), and is presented in Fig. 3. Since the carbonation within the samples varied from the surface to the centre, the specimen were milled and mixed prior to

TGA analysis. The results, thus, represent the average extent of carbonation in the overall sample under each condition. In general, it appears from Fig. 3 that, the degree of carbonation of the samples increases steadily with age in the carbonation chamber, and with the increase of pressure, temperature and duration in the carbonation reactor. In the carbonation chamber, similar to the compressive strength gain, the CO_2 uptake increases approximately linearly with time (Fig. 3a). In the reactor, with the increase in pCO_2, a steep increase in the CO_2 uptake was observed between 4 and 8 bar. Further increase in pressure to 12 bar did not increase the CO_2 uptake substantially (Fig. 3b). Beyond 12 bar, linear improvement in CO_2 uptake was again observed. This trend differs from that of the strength tests, where higher pressures resulted in a decreased compressive strength of the cubes.

Increase in temperature from 20 to 40 °C did not result in a noticeable increase in CO_2 uptake, which is in line with the results of compressive strength, but thereafter the CO_2 uptake increased linearly (Fig. 3c). In terms of the duration of carbonation in the reactor, the CO_2 uptake improved substantially as a function of time; this is in line with the compressive strength development (Fig. 3d).

In summary, in the carbonation chamber the highest amount of CO_2 sequestration was 4.3 wt.%, achieved after 3 weeks, while the maximum CO_2 sequestration achieved in the carbonation reactor was 8.1 wt.%, obtained at 8 bar pCO_2, 80 °C, and after 15 hours of carbonation. Interestingly, the compressive strength of the samples also showed an almost two-fold increase between the two tested conditions.

The DTG of the carbonated samples is plotted in Fig. S5 (in the Supplementary material). The most evident peak is that in the range 750-800 °C, representing decarbonation (thermal loss of CO_2) of calcite. Two other smaller and broader peaks can also be observed, one near 100 °C, representing dehydration of C-S-H [29, 30] or residual moisture in the carbonated

samples, and another peak visible more prominently in the samples from the carbonation reactor treated for 5 and 15 hours, just prior to 600 °C, likely representing decomposition of $MgCO_3$. It is interesting to note that as the reaction progresses in the carbonation chamber, the calcite peaks shifts towards the right. Similar shifts can also be observed for carbonation in the reactor with increase in CO_2 pressure, temperature and duration of carbonation.

3.4 Porosity and pore structure

Open porosity is one of the important factors determining the physical strength of building materials [31]. To study the effect of carbonation conditions on open porosity of the cubes, the carbonated specimens were analysed. The porosity of the carbonated specimen is expected to vary along the depth of the sample, but since the tests were performed on entire specimen, the results represent an average porosity value for that sample. The pattern in Fig. 4 shows that the open porosity of the specimen prepared in the carbonation chamber for 3 days (35.7%) decreases (to 33.9%) after 3 weeks. Increase in CO_2 pressure in the carbonation reactor from 8 to 20 bar resulted in a minor decrease in porosity. This is in good agreement with the strength and CO_2 uptake results, implying that a high amount of carbonate precipitation induces pore densification and strength gain of the system. The most significant decrease in porosity (from 32.8% to 28.5%) was recorded when the duration of carbonation was increased from 2.5 h to 15 h in the reactor under 8 bar pCO_2 and at 80 °C. The open porosity results largely follow the trends from the compressive strength results.

The pore size distribution of the carbonated specimen, determined by MIP, is shown in Fig. 5. A representative scheme of the specimen used for MIP measurement is also shown in the figure. The results reveal that the sample carbonated in the chamber for 3 days has not only higher pore volume but also larger pores which are depicted by the steeper curve. In comparison, the 3 weeks sample showed a gentler curve, representing the presence of smaller

pores. In the carbonation reactor, increase in CO_2 pressure from 8 to 20 bars at 20 °C did not result in any noticeable change in the porosity of the specimen. Increase in the temperature to 80 °C resulted in a substantial decrease in the pore volume and size due to enhanced carbonation. A similar pattern was observed when the duration of carbonation was increased in the pressurised reactor.

3.5 Quantitative phase analysis

The quantitative mineral phase analysis of the different carbonated samples compared with the fresh slag is shown in Fig. 6. The XRD pattern for the uncarbonated and carbonated AODNS_500, is shown in Fig. S6 (in the Supplementary materials). The most noticeable aspect of the analysis is the increase in the amount of amorphous material in the carbonated slag under all conditions of carbonation. Minerals such as periclase, cuspidine, bredigite, merwinite, β-C_2S and γ-C_2S, show reduction in quantities to varying degrees, whereas calcite appears as the only crystalline calcium carbonate polymorph in the carbonated samples. Less stable calcium carbonate polymorphs of aragonite and vaterite were not resolved by QXRD although their formation cannot be ruled out considering the original phase compositions (Ca- and Mg-silicates) and intensified carbonation conditions [12]. For the carbonation in the CO_2 chamber, after 3 weeks the relative decrease in the quantities of merwinite, β-C_2S, bredigite, cuspidine, γ-C_2S and periclase were, respectively, 69%, 65%, 42%, 30%, 28% and 27%, compared to the composition of the fresh AODNS_500 slag. For the carbonation in the pressurised reactor at 20 °C, 8 bar pCO_2, and after 2.5 h duration, the reduction in mineral content compared to the original slag for merwinite, cuspidine, bredigite, γ-C_2S, β-C_2S and periclase were, respectively, 59%, 30%, 25%, 25%, 24% and 19%, and improved to 61%, 38%, 37%, 30%, 33% and 34% at 20 bar. An increase in temperature from 20 to 80 °C also induced an improvement in carbonation conversion with reduction in the quantities of merwinite, cuspidine, bredigite, γ-C_2S, β-C_2S and periclase by, respectively, 60%, 37%, 48%,

31%, 53% and 52%. Increased duration of carbonation also resulted in further reduction in the quantities of the alkaline earth mineral phases. Although the trend of the results seems to be in line with the TGA data, the amounts of crystalline carbonate products quantified differend considerably from what would be expected based on the CO_2 uptake results.

3.6 FT-IR analysis

The results of the FT-IR analysis of carbonated slag specimen samples compared against fresh slag are shown in Fig. S7 (in the Supplementary materials). Since AODNS slag is composed of a mixture of several minerals, the peak assignment can be complicated because of the possibility of peak overlap. Nevertheless, a distinct peak can be observed in the carbonated samples at 1400-1450 cm^{-1}, which is typically associated with the asymmetric stretching of carbonate ions [32]. The peaks in the region of 800–1200 cm^{-1} correspond primarily to the asymmetric and symmetric stretching vibrations of Si–O bonds [33]. For better identification of the peaks, deconvolution of the FT-IR spectra was done, which is shown in Fig. 7. It is apparent that many new peaks appear after the carbonation of the slag (Fig. 7b). In the fresh AODNS_500 slag (Fig. 7a), the peak close to 650 cm^{-1} (Si-O bending) and the one at 915 cm^{-1} can be attributed to cuspidine; the one around 965 cm^{-1} to bredigite; at 945 and 1025 cm^{-1} to merwinite; at 848, 906 and 936 cm^{-1} to β-C_2S; and at 815 and around 865 cm^{-1} can be assigned to γ-C_2S [34-37]. The small peak at 1060 cm^{-1} can be associated with C-S-H which might have formed due the partial hydration of hydraulic β-C_2S [32]. A suitable match for additional peaks could not be found in literature. In the carbonated slag specimens, depletion in some of the original phases and emergence of some new phases can be observed. Apart from the peaks observed in the fresh slag, the major peaks that appear at 1410 and at 875 cm^{-1}correspond to calcite; the one at 715 cm^{-1} correspond to aragonite; at 1083 cm^{-1} to vaterite and the peak at 1471 cm^{-1} can be associated with either aragonite or

magnesite ($MgCO_3$) [32, 34, 38]. Here also suitable match for several peaks could not be established from available literature.

3.7 Morphology of the carbonated slag

The morphology at the carbonated outer edge of the specimens is shown in Fig. 8. The images indicate presence of calcium carbonate polymorphs (calcite, aragonite and vaterite) in different morphologies, calcite being the predominant polymorph detected by QXRD and FTIR analyses. The samples carbonated in the CO_2 chamber presented a predominantly micrometer-sized irregular morphology, which is expected to be calcite since room temperature and low pCO_2 as well as pH close to neutrality and pH>11 typically favour the development of calcite crystals [39]. The ones from the reactor had cylindrical spindle/flower bud-like structures. The morphology at the outer edge of the carbonated cubes after 3 days of carbonation in the chamber (Fig. 8a) appears to be very similar to that after 3 weeks of carbonation (Fig. 8b), except that the carbonate crystals were scarcer and more scattered at 3 days, whereas they were more abundant and densely packed at 3 weeks. Also, conical spiked crystals resembling aragonite needles could be observed after 3 weeks of carbonation in the CO_2 chamber (Fig 8b, inset).

As for specimens carbonated in the pressurised reactor, although spindle/bud-like crystals were commonly seen at the outer edge of the specimens, the sample carbonated for 2.5 h at 20 °C, 8 bar pCO_2 (Fig. 8c) showed a differently featured morphology which appears more eroded than the other samples. In the reactor, at higher operating temperatures (80 °C), the crystals resemble a less common form of football-shaped calcite, elongated along the *c* axis, which is typically formed at high temperature and high supersaturation [39] as well as in the presence of ionic additives such as Mg^{2+} [40]. Eroded surface features of these calcite crystals seem to indicate their dissolution under prevailing operating conditions of high

relative humidity and *p*CO2, the latter leading to pH drop with further dissolution of CO_2 [41].

Besides calcite, in the sample carbonated for 2.5 h at 20 °C and 20 bar pCO_2 (Fig. 8d), some rod/needle-like aragonite particles were visible [42, 43], and in the sample carbonated for 2.5 h at 80 °C and 8 bar pCO_2 (Fig. 8e), dumbbell-like aragonite morphologies [44] at the tips of slag particles could also be seen at select locations. Aragonite formation can be attributed to elevated temperatures and presence of Mg^{2+} ions in the slag composition [39, 45]. Nano sized spherical particles resembling vaterite were detected occasionally when carbonation was carried out at higher pressures and temperature (Fig.8 d,e,f). Vaterite is usually unstable at room temperature and pressure [30]. The synthetic phase of vaterite can occur when formation of calcite and aragonite is chemically inhibited for some reason [46]. Some striated morphologies of carbonated slag were also observed after 15 h of carbonation in the reactor at 80 °C and 8 bar pCO_2 (Fig. 8f inset).

Since carbonation reaction in the compacted specimens evolves from the surface inwards via CO_2 diffusion through the open pore system, the progress of carbonation created two distinct zones in the carbonated cubic specimens. These were more visible in the samples prepared in the reactor. In Fig. S8 (in the Supplementary materials), these zones have been outlined. In the samples from the reactor, the inner material was substantially softer than the outer material, as it could be easily scratched by hand. The only exception to this was the sample carbonated at 80 °C, 8 bar pCO_2, for 15 h (second cube on second row of Fig. S8),where these distinct zones could not be observed, but instead a faint division could be seen about 0.5 cm from the outer edge. For the samples prepared in the carbonation chamber, after 3 days a faint zone was visible (third cube, first row), but the material was found to be harder (i.e. could not be easily scratched) than the reactor samples. After 3 weeks of carbonation in the CO_2 chamber, no such zone was visible (third cube, second row).

SEM investigation of the interior of the cubes showed a difference in morphology of the carbonated material within the samples. An example in Fig. 9 shows the difference in the morphology of a carbonated specimen at the outer edge, at approximately 1 cm from the outer edge, and at the centre of the cube. It can be observed that, compared to the bud-like carbonate crystal structure observed on the outer edge, the morphology of carbonated particles inside the cube appear more similar to that observed on the outer edge of specimens from the carbonation chamber (Fig. 8 a, b). In Fig. S9 (in the Supplementary materials), a zone could be observed where on the right-hand side the carbonated particles appear more rounded, whereas on the left-hand side they appear as small precipitated particles of varying sizes joined together. At the centre of the sample (Fig. 9c), not only were the carbonate crystals less abundant, but also the slag particles appeared to be more loosely attached to each other. This is due to the fact that the carbonated outer edge of the specimen becomes too dense to allow CO_2 diffusing into the centre, as inferred from the phenolphthalein spray tests. Similar differences in morphology could be seen in all the samples prepared in the carbonation reactor (not shown). A possible explanation can be the fact that intensified carbonation under the investigated pressurized conditions causes capillary condensation which blocks the capillary pore disabling CO_2 diffusion. For the samples prepared in the carbonation chamber, no difference in morphology could be observed between the exterior and interior structure (not shown).

To observe the carbonation reaction diffusion front in the carbonated specimens, elemental mapping was performed on resin-impregnated polished samples. In Fig. 10, a map is shown as an example for the sample carbonated for 3 weeks in the carbonation chamber. The intense red colour in the Ca and Si maps show unreacted phases in the slag. The green coloured rims around the grains represent the carbonation of the calcium silicate phases. In the C map, the white areas show the pores in the sample whereas the dark patches show unreacted slag

particles. The green coloured areas show the places where carbonation reaction has taken place. Isolated MgO and CaF_2 particles are also visible in the matrix with rims of lower intensity colour, suggesting initiation of carbonation reactions around these particles. The elemental maps of Ca, Mg and C for the other specimens are presented in Fig. S10 (in the Supplementary materials). The presence of rims of lower intensity around the particles is evidence of the fact that the carbonation reaction of the constituent slag particles occurs via diffusion/precipitation process. Other researchers have also mentioned similar mechanism where the carbonation reaction is governed by calcite precipitation on the particle surfaces and that the reaction rate is determined by the degree of ion diffusion through the solid matrix [21, 27].

3.8 pH and leaching of heavy metals

The pH of fresh AODNS_500 slag and the crushed carbonated specimens after 24 h batch leaching tests is shown in Fig. 11. Carbonation caused a decrease in the pH of the material up to 1 unit, and the pattern of decrease in pH was very similar to the TGA results of these samples (Fig. 3). Increased time of carbonation in the CO_2 chamber and increase of pressure, temperature and duration in the pressurised reactor all caused a reduction of the pH in the solutions of the carbonated samples.

The heavy metal and metalloid leaching from the carbonated samples was compared to the current leaching limits established in Wallonia, Belgium for waste materials re-use presented in Table 3 [47]. The leaching values for As, Co and Mo were below the detection limit of the ICP-MS. The results for the remaining elements have been plotted in Fig. 12. The solid line represents the prescribed limits. In the cases where limits are non-regulated or are too high to be indicated within the y-axis range, no line has been marked. With respect to the non-regulated heavy metals, V showed an increase in leaching with increasing carbonation (and

consequently decreasing pH), whereas leaching of Ba decreased proportional to the extent of carbonation. Compared to the regulated leaching limits, all elements except Cr were below the prescribed limits. The leaching of Cu, Pb, Se and Ti displayed no significant change after carbonation. The leaching of Ni and Zn were reduced as a result of carbonation. The leaching of Cr showed fluctuations, with some samples meeting the imposed limits, and others exceeding. The Cr leaching from the fresh AODNS_500 slag was found to be higher than the prescribed limit. The Cr leaching fell below the limit during initial carbonation in the chamber for 3 days and in the reactor at 8 bar pCO_2, 20 °C, for 2.5 h. Further carbonation in the CO_2 chamber for 3 weeks or increase in pressure and temperature in the pressurised reactor resulted in an increase of Cr leaching beyond the prescribed limit. A decrease in Cr leaching was observed again as the carbonation duration in the reactor was increased to 15 h.

4. Discussions

The carbonation process of alkaline silicates includes three principle reactions: dissolution of alkaline earth metals, hydration and dissolution of CO_2, and precipitation of carbonates. Under ambient conditions, dissolution of CO_2 gas in water, leading to the formation of carbonic acid (H_2CO_3), is described as the slowest and the rate determining step. This reaction is followed by ionisation of H_2CO_3 to HCO^{3-}, CO_3^{2-} and H^+ ions, which comparatively occurs almost instantaneously. Subsequently, reaction of CO_3^{2-} ions with Ca^{2+} and Mg^{2+} ions leached out from the silicates takes place resulting in the formation and precipitation of Ca- and Mg-carbonates [30, 48]. In the present work the carbonation mechanism differs, since the CO_2 transport to the solid bulk of the cubic specimens is limited due to its physical shape, which controls the diffusion of CO_2 through most of the sample. It therefore becomes difficult for the CO_2 to reach all the slag particles equally, unlike in the case of fine powdered particles in aqueous slurry, as many works have investigated, where all

particles are readily available for carbonation reaction and the rate of which is primarily controlled by the particle surface area. The amount of water in the system can also have an influence on the carbonation of the slag in the cubic specimen as in the presence of excessive water the gaseous CO_2 diffusion/reactivity is retarded and if the moisture is too little, carbonation will not proceed at un-wetted surfaces [30]. Also, since one of the products of carbonation reaction is water and the particles of slag may get submerged, the carbonation reaction will also depend on whether the drying front precedes or follows the wetting front caused by the carbonation reaction [49]. The rate and total uptake of CO_2 will also govern the interstitial geometry of the sample because carbonate precipitation will modify porosity and restrict the further ingress of CO_2 through the open pore network [50].

The reaction in the carbonation chamber at atmospheric pressure is a relatively slow process, compared to that in the pressurised reactor, but the higher than atmospheric CO_2 concentration used in the later (5%) is still able to facilitate accelerated carbonation compared to ambient curing. The increase in duration of carbonation allows more CO_2 to diffuse inside the cubes, and hence more carbonation products to form, which contributes to the mechanical strength gain. Hence, an increase in compressive strength is observed (Fig. 1a). The same mechanism explains the trend observed with regards to CO_2 uptake (Fig. 3a).

In the carbonation reactor, where the CO_2 pressure and temperature was intensified, the reaction kinetics was accelerated further. Hence, increase in pCO_2 to 8 bar resulted in improvement in compressive strength (Fig. 1b). This pattern appears obvious as increase in pressure should force more CO_2 inside the cube, and hence facilitate further reaction, leading to an increase in the CO_2 uptake and the formation of carbonates. The possible reason for the observed decrease in strength at higher pressures can be either because of the rapid formation of carbonates at the outer edge of the specimen, which would limit further diffusion of CO_2 towards the core of the cube, and/or that, since the freshly prepared sample was very soft, an

increase in pressure beyond a limit could introduce micro cracks in the sample, and hence create failure zones in it. Micro cracks can also be induced in the samples due to secondary heating effect in the sample as carbonation reaction is exothermic. If sufficient heat is evolved to vaporise a portion of water present within the samples it can cause steam formation and result in micro-cracking [51]. The vaporisation of water was visualised by the presence of condensed water on the walls of the reactor. These processes may get accelerated at higher pressures and cause strong and weak zones in the same specimen, which can be the reason for the high variation in compressive strength measured for the samples prepared at 20 bar. Since TGA analysis shows an increased CO_2 uptake with an increase in pressure (Fig. 3b) it may be prudent to increase the pressure in steps, to ensure that the sample gets suitable endurance to bear the higher pressures.

Temperature can affect carbonation in two ways: an increase in temperature accelerates the reaction kinetics and hence boosts the CO_2 uptake [48], whereas the CO_2 dissolution decreases with increase in temperature (Henry's Law), which may slow down carbonation reactions. In the present case, it appears that the acceleration of reaction is the dominating factor, and hence increase in compressive strength is observed at elevated temperatures. The huge variation in strength seen at 120 °C might have occurred due to increased evaporation of water from the sample, which might have resulted in non-uniform carbonation of the cubes.

The highest improvement in strength gain and CO_2 uptake was seen by increasing the duration of carbonation in the reactor. The compressive strength of ~60 MPa, which was achieved after 15 h, is more than enough for most uses in the construction industry, though the CO_2 sequestration of 8.1 wt.% is well below the theoretical maximum capacity (34.1 wt.%), and the carbonation levels achieved by researchers utilizing AOD slag in powder form. On a positive note, if such a carbonated cube is used as a building material, then it may continue to act as a carbon sink for atmospheric CO_2 during its lifetime service in

the structure, because of the presence of unreacted alkaline earth metal oxides in it that may continue to react over time.

The results of compressive strength testing show that in a simple set-up, such as the carbonation chamber, more time is necessary to achieve suitable properties, whereas in an intensified set-up, such as the pressurized reactor, it can be achieved in a matter of hours. Simultaneously, formation of C-S-H was observed, represented by the initial peak at 100 °C in the DTG plot (Fig. S5); this has been reported to occur during carbonation of calcium silicate minerals by Bukowski and Berger [30] and Young et. al [52]. Carbonation at higher temperatures and for longer durations in the reactor has an advantage as it promotes the formation of $MgCO_3$, represented by the decomposition peak at 600 °C in Fig. S5. The basic character of CaO is 25-30% greater than MgO [53]. Hence, CaO constitutes a better electron donor and is more reactive than MgO, and so is preferably and relatively more easily carbonated [54]. Carbonation of MgO is advantageous, as delayed hydration of free MgO is known to cause durability issues in building materials [14]. This is therefore another advantage of using the reactor set-up over the carbonation chamber which delivers a milder carbonation yield. On the other hand, not only does the carbonation reactor require a more advanced set-up, it also uses more energy for heating and compression. Since energy can be directly linked to CO_2 emissions, given the current power generation mix, a trade-off must be found between the two methods to select the preferable one. Nevertheless, the results of the compressive strength tests show that carbonated AODNS_500 slag has a very good potential to be used in the fabrication of building materials.

Increased carbonation due to longer carbonation period in the carbonation chamber, as well as an increase of CO_2 pressure, temperature and duration in carbonation reactor, cause densification of the pore structures and hence reduction of open porosity (Fig. 4). The pattern observed is very similar to the TGA results. An almost similar pattern can be seen in MIP

results as well (Fig. 5). The reason for the specimens carbonated in the reactor at 8 and 20 bar showing very similar pore volume can be that at higher pressure the pores get clogged with the reaction products, which can affect the permeability of mercury thorough the pores and hence the MIP results [31]. Another conclusion that can be drawn from Fig. 5 is that, although carbonation in the chamber for 3 days and in the reactor at 8 and 20 bar results in similar pore volumes, the sample prepared in the carbonation chamber had smaller pores (represented by gentler slope). This could be physically observed on the specimen (Fig. S8), since the core of cubes prepared in the reactor (except for the one sample carbonated for 15 h) appeared softer than those from the carbonation chamber.

The QXRD results show that in the carbonated samples an appreciable quantity of material was undetectable due to its poorly crystalline/amorphous nature. The presence of calcite was found to be higher in the samples carbonated in the CO_2 chamber. Amorphicity in the carbonated specimens could have occurred due to several factors. It could have been induced by milling in the ring mill, as mechanical activation is known to reduce crystallinity of minerals [55]. Also, Cizer et. al. [41, 56] have shown that accelerated carbonation results in the formation of amorphous carbonates. Another possibility is that the crystalline calcium and calcium-magnesium silicates after losing Ca ions to carbonation may lose their crystalline nature and form poorly crystalline materials. Huijgen et. al. [27] have reported formation of Ca-depleted SiO_2 phase around calcium silicate minerals as a result of accelerated carbonation. Nevertheless, the QXRD results establish that merwinite, bredigite, γ-C_2S and cuspidine can carbonate to varying degrees under different conditions, whereas carbonation of periclase, as confirmed by DTG, is feasible when carbonation is carried out at higher temperatures for longer times. In general, merwinte was the mineral phase most prone to carbonation by both processes in all conditions. γ-C_2S was found to be least reactive in the reactor and periclase least reactive in the carbonation chamber. Working with pure minerals,

Bodor et. al. [57] have reported that synthetically generated bredigite is the most reactive of among seven synthesised steel slag phases. Santos et. al. [12] found that C_2S polymorphs are more prone to carbonation whereas cupidine, merwinite and periclase perform poorly under thin film carbonation of stainless steel slags. They also report that under slurry carbonation, β-C_2S and γ-C_2S react more readily whereas the carbonation of bredigite, cuspidine and periclase improve at extended processing times. Hence, the carbonation extent of the individual minerals in the slag varies depending upon the method as well as the processing conditions.

Although calcite was the only carbonate phase detected by XRD, FT-IR analysis showed the presence of other phases of Ca and Mg-carbonates in the samples. It is possible that the crystal domains of these carbonated phases were too small and hence undetectable for a technique like XRD that probes long range order, but detectable by FT-IR that looks into the local bonding environment. FT-IR has the capability of detections at much lower concentrations, since the carbonated group has high dipolar moment, whereas for XRD the phases need to be present in the range of at least 1-2 wt% to ascertain their presence in the material.

The existence of amorphous material found by QXRD analysis is supported by the presence of tiny and irregularly shaped carbonate crystals seen in the SEM images (Fig. 8a, 8b and 9). Another conclusion that can be drawn from the SEM analysis is that rapid carbonation under the influence of higher pressures and temperatures promotes the formation of flower bud/football-like calcite at the outer edges of the specimens carbonated in the reactor. As the CO_2 penetrates further, its diffusion slows down, resulting in the formation of tiny and irregular calcite particles. The same phenomenon is responsible for the morphology of calcite in the carbonation chamber where the diffusion of CO_2 is slower since the process is carried out at atmospheric pressure and dilute CO_2 concentrations.

With regards to the leaching of hazardous elements, the leaching of V was seen to increase after carbonation. Increase in V leaching in slags and MSWI-BA has been documented by others as well [18, 19, 21]. This element is currently not included in the regulations referred in this work, but if its future leaching limit value is similar to those of other currently regulated metalloids (i.e. 1–2 mg/kg), it still would not pose a leaching threat as its leaching values remained relatively low (0.5 mg/kg at most). Also, a drop in leaching after 15 h of carbonation in the reactor shows that extended carbonation could contain V leaching. The decrease in the leaching of Zn and Ba as observed in the current study has also been reported elsewhere for steel slags [12, 18]. The variable pattern of Cr leaching (the only regulated element posing a leaching threat) may be related to several parameters such as the presence of C-S-H, pH change, modification of pore structure, and the precipitation of double salts [48]. Van Gerven et. al. [58] have also reported that the effect of carbonation on the Cr leaching of MSWI-BA was unclear. Santos et. al. [12] found that under extended carbonation of steel slags in a slurry reactor, when pH drops below 10.5, reduction in Cr leaching from AODNS slag is observed. This can explain the lowering of leaching in the samples carbonated in the reactor for 15 h.

5. Conclusions

Argon Oxygen Decarburization (AOD) stainless steel slag in its powdered form (without boron addition), has limited valorisation potential and is a burden in terms of disposal costs. Its high surface area and alkaline properties, on the other hand, give it high potential to act as a carbon sink via mineral carbonation, and if used in the fabrication of building materials such as construction blocks as shown in the present study, can be further valorised. The resulting high value application of the carbonated blocks can make the mineral sequestration of CO_2 more attractive, which is otherwise currently limited due to the energy and capital intensive approaches of previous works, where the resulting carbonated materials are of no or

very low economic value. The results from the current work show that the resulting carbonated material has the required compressive strength needed for most building applications which can be further enhanced by optimising the processing conditions. In spite of gaining the required mechanical strength, the carbonation extent achieved accounts for only a fraction of the total carbonation potential of the slag. The accelerated carbonation of the slag resulted, partly, in the formation of amorphous carbonates and the morphology of the carbonated material was dependent on the processing conditions. The leaching of all heavy metals and metalloids, except in some instance of chromium, was within the prescribed limits.

Acknowledgements

The KU Leuven Industrial Research Fund (IOF) is gratefully acknowledged for funding the Knowledge Platform on Sustainable Materialization of Residues from Thermal Processes into Products (SMaRT-Pro^2) in which this work was performed. The KU Leuven Department of Earth and Environmental Sciences is acknowledged for the use of XRD equipment. Support from the Hercules Foundation (project ZE09-09) is also gratefully acknowledged.

Appendix A. Supplementary materials

References

[1] IPCC, IPCC Special Report on Carbon dioxide Capture and Storage, in, Geneva, Switzerland, 2005.

[2] K.S. Lackner, D.P. Butt, C.H. Wendt, Progress on binding CO2 in mineral substrates, Energy Conversion and Management, 38, Supplement (1997) S259-S264.

[3] IEA, Tracking Clean Energy Progress, in, International Energy Agency, Paris, 2013.

[4] E.E. Chang, C.-H. Chen, Y.-H. Chen, S.-Y. Pan, P.-C. Chiang, Performance evaluation for carbonation of steel-making slags in a slurry reactor, Journal of Hazardous Materials, 186 (2011) 558-564.

[5] E.E. Chang, A.-C. Chiu, S.-Y. Pan, Y.-H. Chen, C.-S. Tan, P.-C. Chiang, Carbonation of basic oxygen furnace slag with metalworking wastewater in a slurry reactor, International Journal of Greenhouse Gas Control, 12 (2013) 382-389.

[6] R.M. Santos, D. Ling, A. Sarvaramini, M. Guo, J. Elsen, F. Larachi, G. Beaudoin, B. Blanpain, T. Van Gerven, Stabilization of basic oxygen furnace slag by hot-stage carbonation treatment, Chemical Engineering Journal, 203 (2012) 239-250.

[7] R. Baciocchi, G. Costa, E. Di Bartolomeo, A. Polettini, R. Pomi, Carbonation of Stainless Steel Slag as a Process for CO_2 Storage and Slag Valorization, Waste and Biomass Valorisation, 1 (2010) 467-477.

[8] R. Baciocchi, G. Costa, E. Di Bartolomeo, A. Polettini, R. Pomi, Wet versus slurry carbonation of EAF steel slag, Greenhouse Gases: Science and Technology, 1 (2011) 312-319.

[9] Y.J. Kim, I. Nettleship, W.M. Kriven, Phase Transformations in Dicalcium Silicate: II, TEM Studies of Crystallography, Microstructure, and Mechanisms, Journal of the American Ceramic Society, 75 (1992) 2407-2419.

[10] A. Seki, Y. Aso, M. Okubo, F. Sudo, K. Ishizaka, Development of Dusting Prevention Stabilizer for Stainless Steel Slag, in, 1986, pp. 16-21.

[11] D. Durinck, F. Engström, S. Arnout, J. Heulens, P.T. Jones, B. Björkman, B. Blanpain, P. Wollants, Hot stage processing of metallurgical slags, Resources, Conservation and Recycling, 52 (2008) 1121-1131.

[12] R.M. Santos, J. Van Bouwel, E. Vandevelde, G. Mertens, J. Elsen, T. Van Gerven, Accelerated mineral carbonation of stainless steel slags for CO2 storage and waste valorization: Effect of process parameters on geochemical properties, International Journal of Greenhouse Gas Control, 17 (2013) 32-45.

[13] R.M. Santos, D. François, G. Mertens, J. Elsen, T. Van Gerven, Ultrasound-intensified mineral carbonation, Applied Thermal Engineering, 57 (2013) 154-163.

[14] F. Lea, Chemistry of Cement and Concrete, 4th ed., John Wiley & Sons, New York, 1998.

[15] J.S.J. van Deventer, J.L. Provis, P. Duxson, D.G. Brice, Chemical research and climate change as drivers in the commercial adoption of alkali activated materials, Waste and Biomass Valorisation, 1 (2010) 145-155.

[16] The World Business Council for Sustainable Development,www.wbcsd.org., in.

[17] WBCSD, Cement Technology Roadmap 2009 - Carbon emissions reductions up to 2050, in, 2009.

[18] P. Suer, J.-E. Lindqvist, M. Arm, P. Frogner-Kockum, Reproducing ten years of road ageing — Accelerated carbonation and leaching of EAF steel slag, Science of The Total Environment, 407 (2009) 5110-5118.

[19] R.M. Santos, G. Mertens, M. Salman, Ö. Cizer, T. Van Gerven, Comparative study of ageing, heat treatment and accelerated carbonation for stabilization of municipal solid waste

incineration bottom ash in view of reducing regulated heavy metal/metalloid leaching, Journal of Environmental Management, 128 (2013) 807-821.

[20] G. Cornelis, T.V. Gerven, C. Vandecasteele, Antimony leaching from MSWI bottom ash: Modelling of the effect of pH and carbonation, Waste Management, 32 (2012) 278-286.

[21] A. van Zomeren, S.R. van der Laan, H.B.A. Kobesen, W.J.J. Huijgen, R.N.J. Comans, Changes in mineralogical and leaching properties of converter steel slag resulting from accelerated carbonation at low CO2 pressure, Waste Management, 31 (2011) 2236-2244.

[22] A.A. Coelho, Topas Academic v4.1, <http://members.optusnet.com.au/alancoelho/>, (2007).

[23] R.W. Cheary, A. Coelho, A fundamental parameters approach to X-ray line-profile fitting, Journal of Applied Crystallography, 25 (1992) 109-121.

[24] EN1097-6, Tests for mechanical and physical properties of aggregates – Part 6: Determination of particle density and water absorption, in, 2000.

[25] EN 196-1:1994 Methods of testing cement - Part 1: Determination of strength.

[26] H.H. Steinour, Some effects of carbon dioxide on mortars and concrete, American Concrete Institute, 30 (1959) 905-907.

[27] W.J.J. Huijgen, R.N.J. Comans, Mineral CO2 Sequestration by Steel Slag Carbonation, Environmental Science & Technology, 39 (2005) 9676-9682.

[28] E. Verstrynge, Long-term behaviour of monumental masonary constructions: modelling and probabilistic evaluation, in: Department of civil engineering, KU Leuven, Leuven, 2010.

[29] G.W. Groves, A. Brough, I.G. Richardson, C.M. Dobson, Progressive Changes in the Structure of Hardened C3S Cement Pastes due to Carbonation, Journal of the American Ceramic Society, 74 (1991) 2891-2896.

[30] J.M. Bukowski, R.L. Berger, Reactivity and strength development of CO2 activated non-hydraulic calcium silicates, Cement and Concrete Research, 9 (1979) 57-68.

[31] H. Taylor, Cement Chemistry, 1st ed., Academic Press Limited, London, 1990.

[32] P. Yu, R.J. Kirkpatrick, B. Poe, P.F. McMillan, X. Cong, Structure of Calcium Silicate Hydrate (C-S-H): Near-, Mid-, and Far-Infrared Spectroscopy, Journal of the American Ceramic Society, 82 (1999) 742-748.

[33] C. Alonso, C. Andrade, L. Fernández, A. Hidalgo, The role of magnesium during the hydration of C3S and C-S-H formation. Scanning electron microscopy and mid-infrared studies, Advances in Cement Research, 17 (2005).

[34] J.A. Gadsden, Infrared Spectra of Minerals and Related Inorganic Compounds, Butterworths, London UK, 1975.

[35] S.M. Mirhadi, F. Tavangarian, R. Emadi, Synthesis, characterization and formation mechanism of single-phase nanostructure bredigite powder, Materials Science and Engineering: C, 32 (2012) 133-139.

[36] A. Cruz-Ramírez, J. Romo-Castañeda, M.d.l.Á. Hernández-Pérez, M. Vargas-Ramírez, A. Romero-Serrano, M. Hallen-López, An application of infrared analysis to determine the mineralogical phases formation in fluxes for thin slab casting of steel, Journal of Fluorine Chemistry, 132 (2011) 323-326.

[37] S.N. Gosh, IR Spectroscopy, in: V.S. Ramachandran, J.J. Beaudoin (Eds.) Handbook of analytical techniques in concrete science and technology, Noyes Publications, New York, 2001.

[38] S.D. Škapin, I. Sondi, Synthesis and characterization of calcite and aragonite in polyol liquids: Control over structure and morphology, Journal of Colloid and Interface Science, 347 (2010) 221-226.

[39] C.Y. Tai, F.B. Chen, Polymorphism of CaCO3, precipitated in a constant-composition environment, AIChE Journal, 44 (1998) 1790-1798.

[40] D. Kralj, J. Kontrec, L. Brecević, G. Falini, V. Nöthig-Laslo, Effect of inorganic anions on the morphology and structure of magnesium calcite, Chemistry, 10(7) (2004) 1647-1656.

[41] Ö. Cizer, C. Rodriguez-Navarro, E. Ruiz-Agudo, J. Elsen, D. Gemert, K. Balen, Phase and morphology evolution of calcium carbonate precipitated by carbonation of hydrated lime, Journal of Materials Science, 47 (2012) 6151-6165.

[42] R.M. Santos, P. Ceulemans, T. Van Gerven, Synthesis of pure aragonite by sonochemical mineral carbonation, Chemical Engineering Research and Design, 90 (2012) 715-725.

[43] G.-T. Zhou, J.C. Yu, X.-C. Wang, L.-Z. Zhang, Sonochemical synthesis of aragonite-type calcium carbonate with different morphologies, New Journal of Chemistry, 28 (2004) 1027-1031.

[44] H. Guo, Z. Qin, P. Qian, P. Yu, S. Cui, W. Wang, Crystallization of aragonite CaCO3 with complex structures, Advanced Powder Technology, 22 (2011) 777-783.

[45] K. Sawada, The mechanisms of crystallization and transformation of calcium carbonates, Pure & Applied Chemistry, 69 (1997) 921-928.

[46] W.D. Carlson, Carbonates: Mineralogy and chemistry, in: R.J. Reeder (Ed.) Reviews in mineralogy. Vol. 11, Mineralogical Society of America, New York, 1983.

[47] M.d.l.R. Wallonne, Arrêté du Gouvernement wallon favorisant la valorisation de certains déchets, in, Moniteur Belge, 2001, pp. 23859–23883.

[48] M. Fernández Bertos, S.J.R. Simons, C.D. Hills, P.J. Carey, A review of accelerated carbonation technology in the treatment of cement-based materials and sequestration of CO2, Journal of Hazardous Materials, 112 (2004) 193-205.

[49] K. Balen, D. Gemert, Modelling lime mortar carbonation, Materials and Structures, 27 (1994) 393-398.

[50] D.C. Johnson, C.L. Macleod, P.J. Carey, C.D. Hills, Solidification of stainless steel slag by accelerated carbonation, Environmental Technology, 24 (2003) 671-678.

[51] W.A. Klemm, R.L. Berger, Accelerated curing of cementitious systems by carbon dioxide: Part I. Portland cement, Cement and Concrete Research, 2 (1972) 567-576.

[52] J.F. Young, R.L. Berger, J. Breese, Accelerated Curing of Compacted Calcium Silicate Mortars on Exposure to CO2, Journal of the American Ceramic Society, 57 (1974) 394-397.

[53] G. Pacchioni, J.M. Ricart, F. Illas, Ab Initio Cluster Model Calculations on the Chemisorption of CO2 and SO2 Probe Molecules on MgO and CaO (100) Surfaces. A Theoretical Measure of Oxide Basicity, Journal of the American Chemical Society, 116 (1994) 10152-10158.

[54] D. Bonenfant, L. Kharoune, S. Sauvé, R. Hausler, P. Niquette, M. Mimeault, M. Kharoune, Molecular analysis of carbon dioxide adsorption processes on steel slag oxides, International Journal of Greenhouse Gas Control, 3 (2009) 20-28.

[55] L. Kriskova, Y. Pontikes, Ö. Cizer, G. Mertens, W. Veulemans, D. Geysen, P.T. Jones, L. Vandewalle, K. Van Balen, B. Blanpain, Effect of mechanical activation on the hydraulic properties of stainless steel slags, Cement and Concrete Research, 42 (2012) 778-788.

[56] Ö. Cizer, K. Van Balen, J. Elsen, D. Van Gemert, Real-time investigation of reaction rate and mineral phase modifications of lime carbonation, Construction and Building Materials, 35 (2012) 741-751.

[57] M. Bodor, R.M. Santos, L. Kriskova, J. Elsen, M.V.G. Vlad, T. , Susceptibility of mineral phases of steel slags towards carbonation: mineralogical, morphological and chemical assessment, European Journal of Mineralogy, 25 (2013) 533-549.

[58] T. Van Gerven, E. Van Keer, S. Arickx, M. Jaspers, G. Wauters, C. Vandecasteele, Carbonation of MSWI-bottom ash to decrease heavy metal leaching, in view of recycling, Waste Management, 25 (2005) 291-300.

List of figures:

Fig. 6. Mineral phase composition of carbonated AODNS_500 slag block specimen, determined by QXRD.

Fig. 7. Deconvolution of the FT-IR spectra of: a) fresh AODNS_500 slag; and b) specimen carbonated in the reactor at 8 bar CO_2, 80 °C for 15 h.

Fig. 8. Morphology of carbonated slag at the outer edge of the carbonated block specimens prepared in: (a) carbonation chamber for 3 days; (b) carbonation chamber for 3 weeks ; (c) reactor at 8 bar CO_2, 20 °C, for 2.5 h; (d) reactor at 20 bar CO_2, 20 °C, for 2.5 h, the yellow arrow shows needle shaped aragonite; (e)reactor at 8 bar CO_2, 80 °C, for 2.5 h, the white arrow shows dumbbell shaped aragonite; (f) reactor at 8 bar CO_2, 80 °C, for 15 h, the black arrows show circular vaterite

Fig. 12. SEM image of block interior carbonated in the reactor at 80 °C, 8 bar CO_2 partial pressure, for 2.5 h; locations a, b and c as shown in Fig. S8.

Fig. 10. Elemental mapping (Ca – calcium, Si – silicon, C – carbon, Mg – magnesium, F – fluorine) of the specimen carbonated for 3 weeks in the carbonation chamber near the outer edge of the block.

Fig. 11. pH of fresh AODNS_500 slag and milled carbonated block specimens.

Fig. 12. Heavy metal and metalloid leaching from fresh AODNS_500 slag and milled carbonated block specimens.

List of Tables

List of supplementary figures

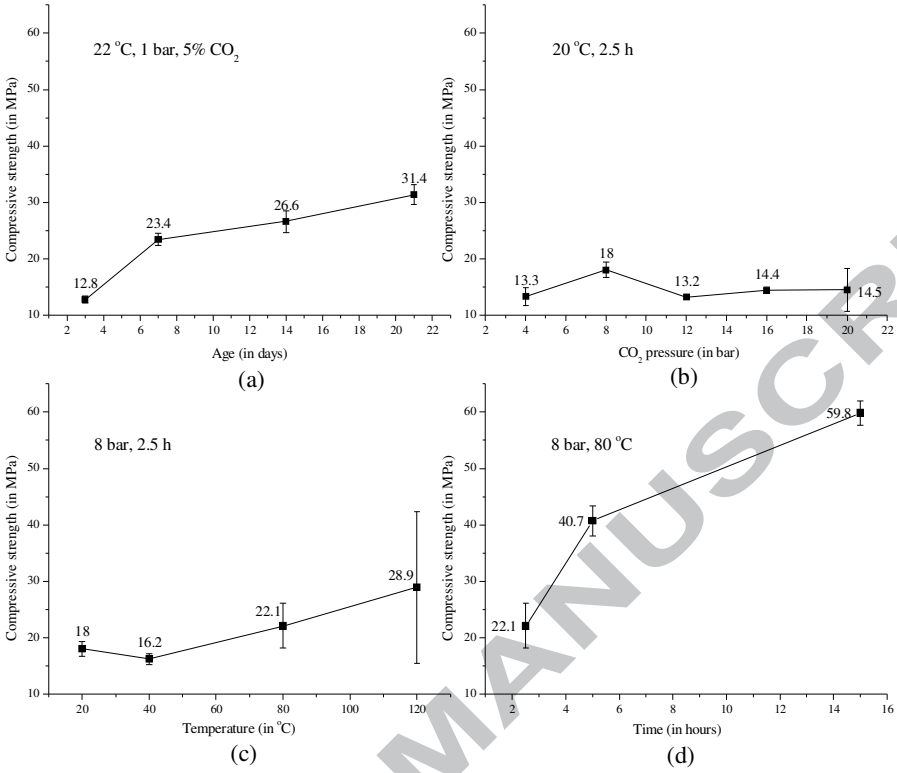

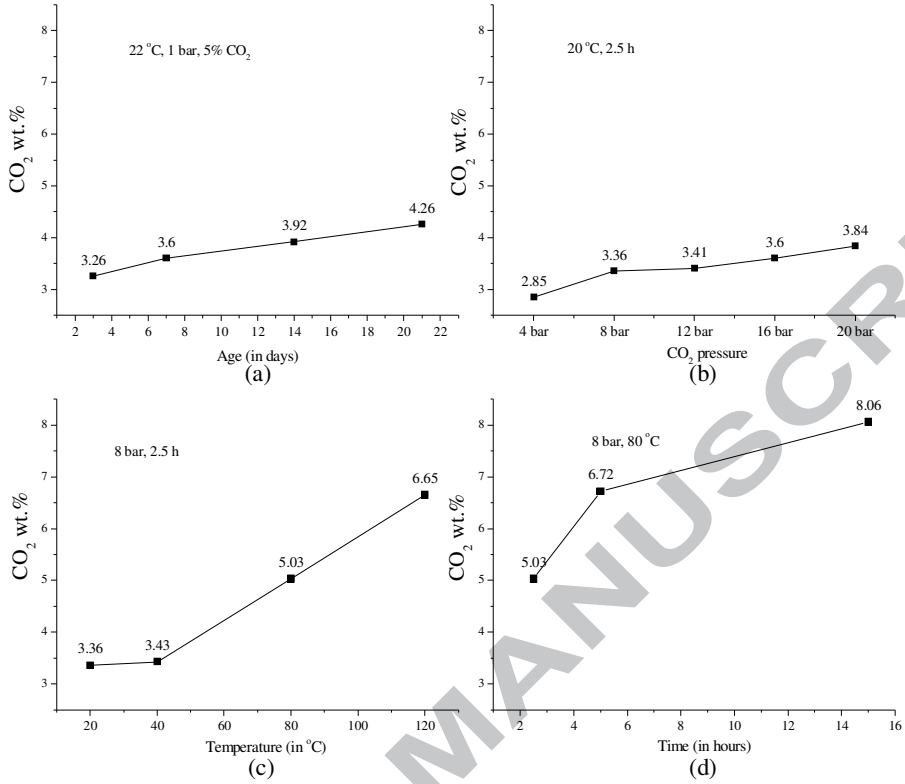

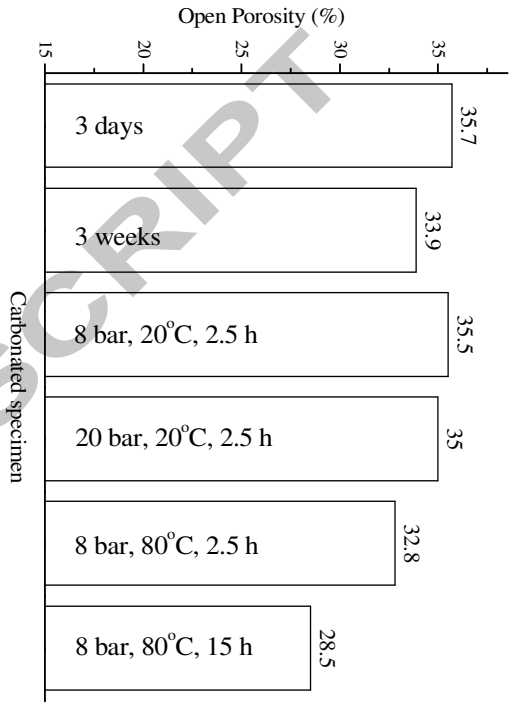

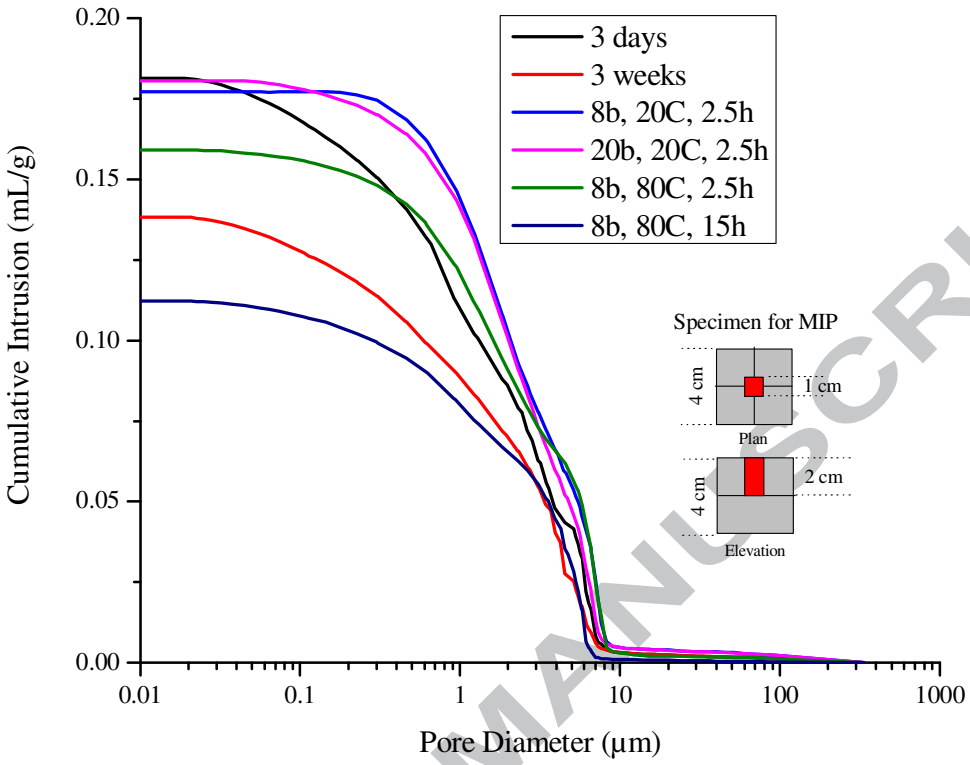

.

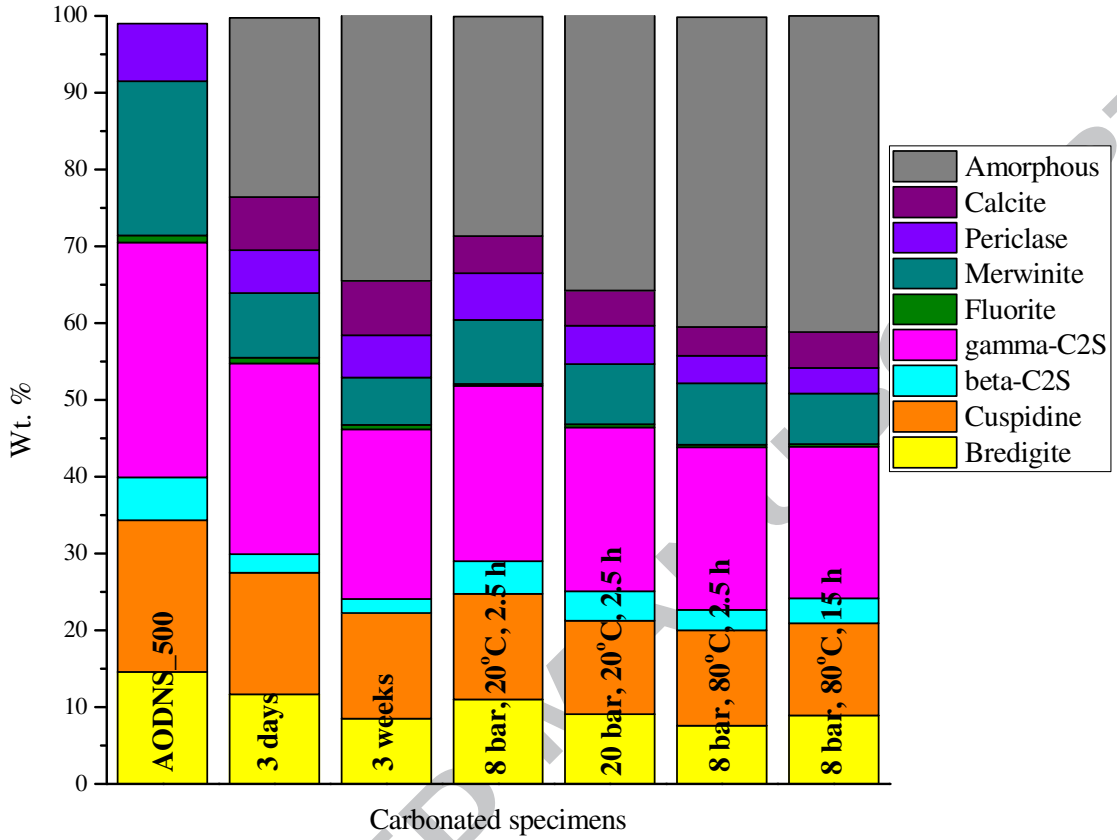

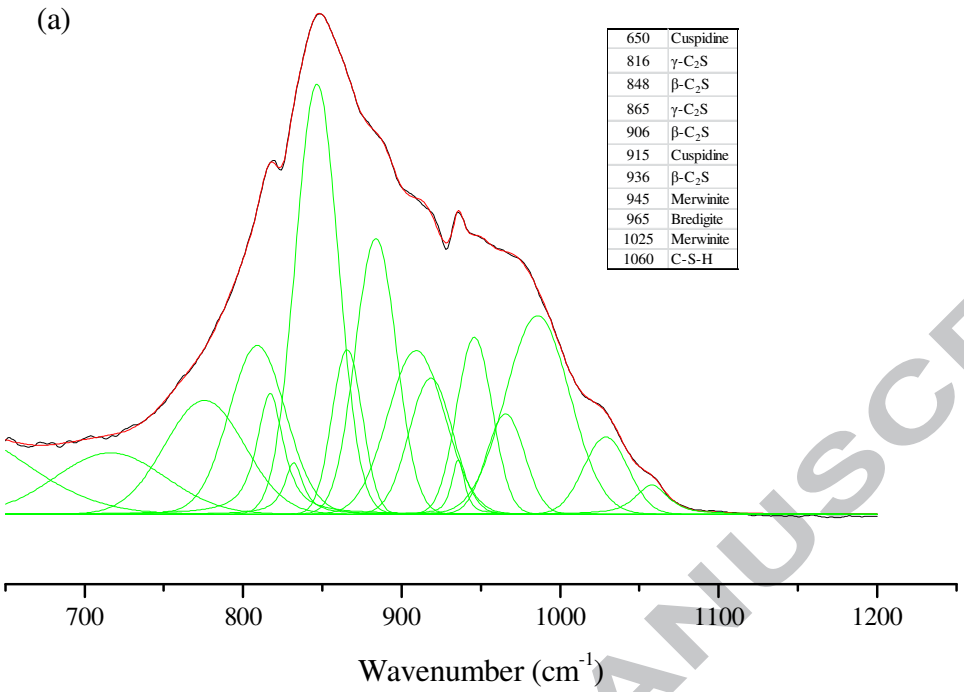

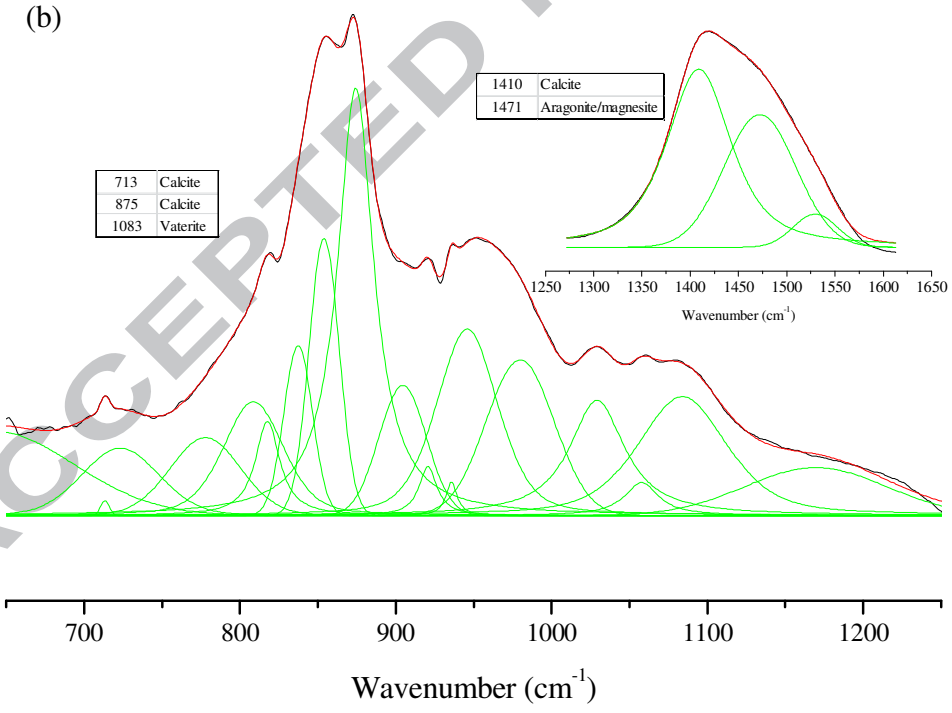

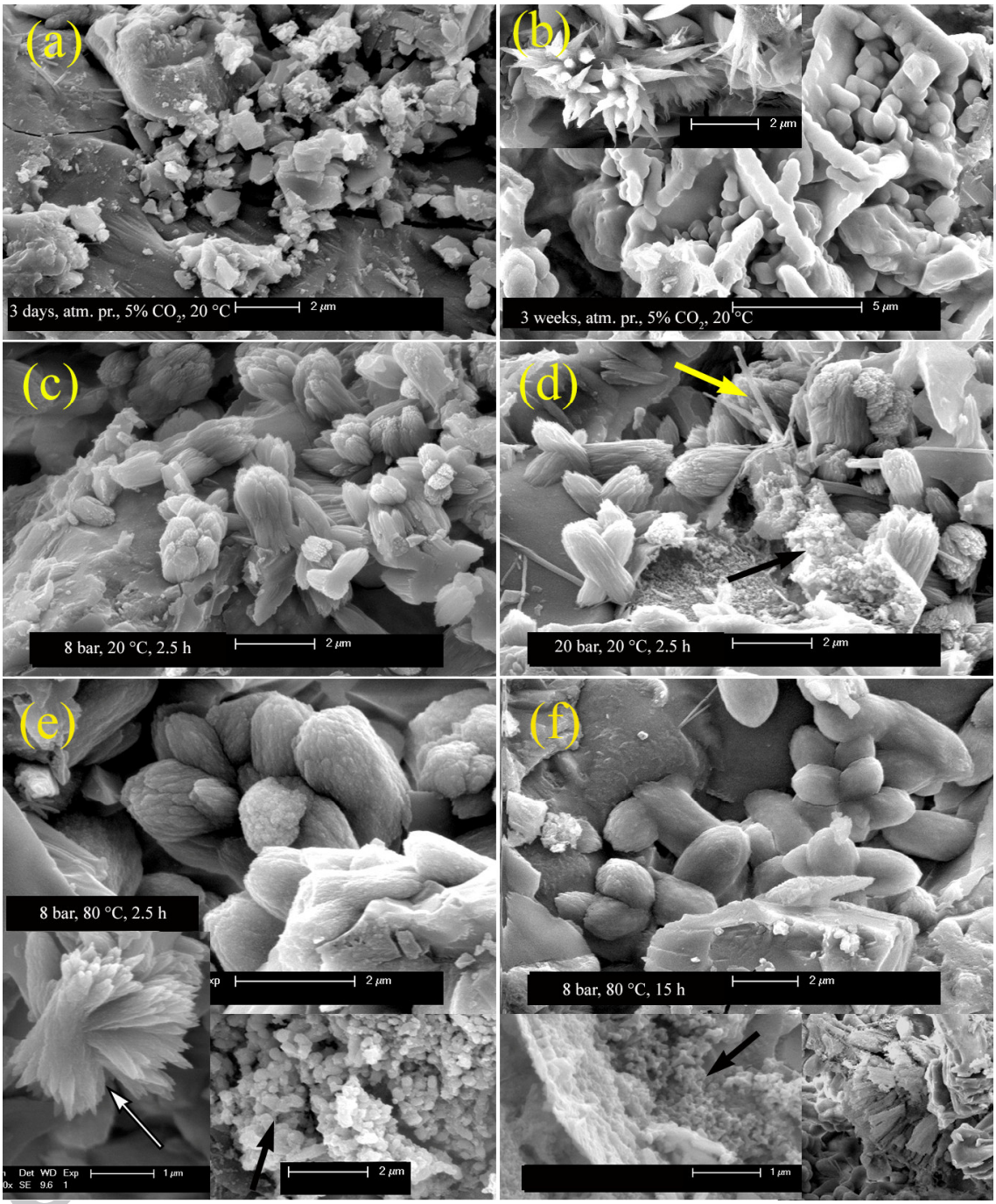

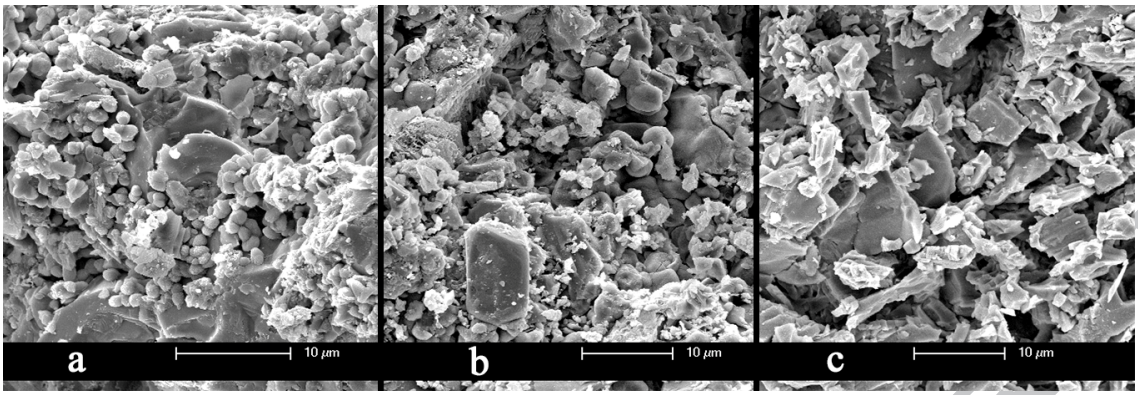

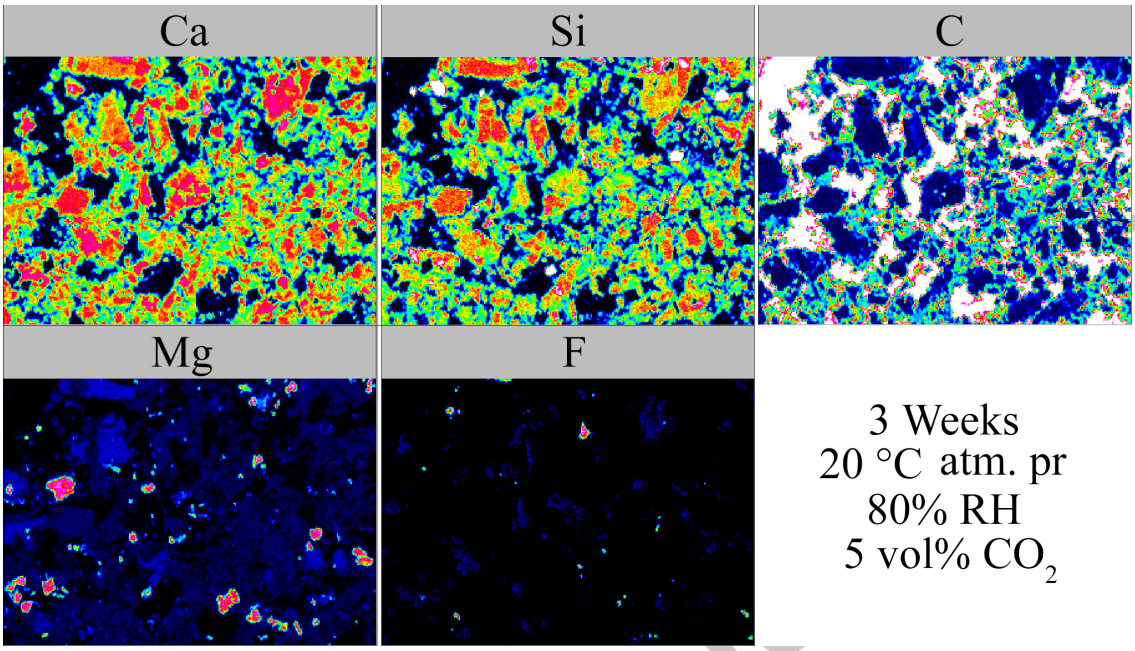

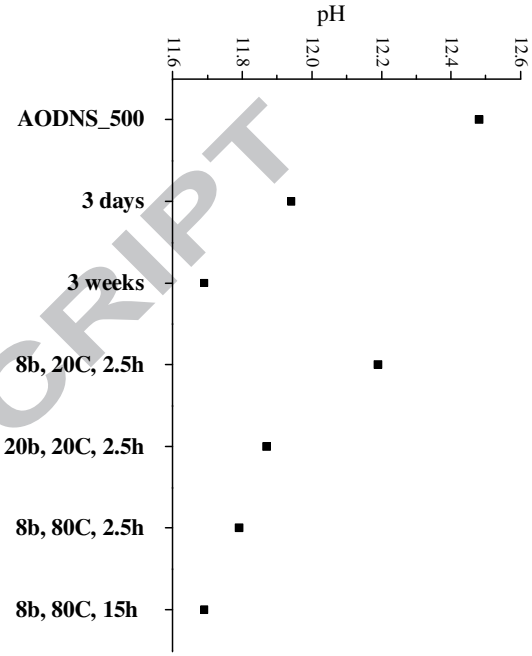

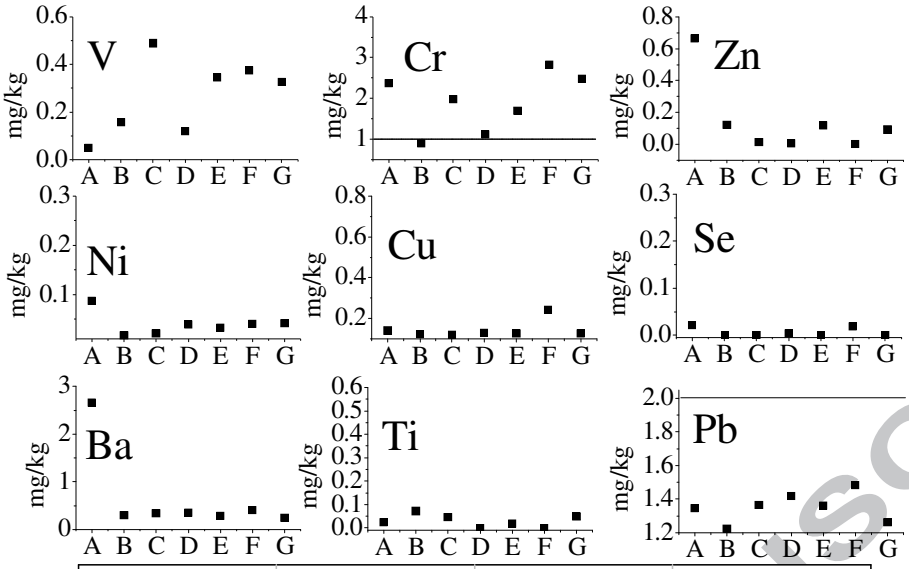

A-AODNS_500	B-3 days	C-3 weeks	D-8b, 20C, 2.5h
	E-20b, 20C, 2.5h	F-8b, 80C, 2.5h	G-8b, 80C,15h

Table 1. Oxide compositions of AODNS_500 by XRF analysis

Oxides	CaO	SiO_2	MgO	Al_2O_3	Cr_2O_3	Fe_2O_3
wt%	**54.5**	34.1	**8.0**	1.1	0.8	0.3

Table 2. Phase composition of AODNS_500 by QXRD analysis

Minerals	Bredigite	Cuspidine	β-C_2S	γ-C_2S	Fluorite	Merwinite	Periclase	Portlandite	Quartz low
wt%	**15**	**20**	6	**30**	1	**20**	7	<1	<1

Table 3. Leaching limits for heavy metals and metalloids regulated in Wallonia, Belgium for waste materials re-use; expressed in mg metals leached per kg material, obtained by 24 h batch shaking test at liquid to solid ratio of 10

	As	Ba	Cd	Co	Cr*	Cu	Mo
Limit (mg/kg)	1.0	NR	1.0	1.0	1.0	20.0	1.5
	Ni	Pb	Sb	Se	Ti	V	Zn
Limit (mg/kg)	2.0	2.0	2.0	NR	20.0	NR	9.0

N. R. : not regulated.

*Limit prescribed for Cr(VI), whereas total Cr measured.

Highlights:

- AOD slag can be valorized as building material by mineral carbonation
- Depending on the process strengths of more than 30 MPa can be achieved
- XRD analysis show formation of amorphous carbonation products
- SEM analysis shows different morphology of calcite at different pressures
- Leaching of several heavy metals is reduced on carbonation